Effect of Structure and Composition of Nanodiamond Powders on Thermal Stability and Oxidation Kinetics

Carlo Bradac[a,*] *and Sebastian Osswald*[b]

[a] School of Mathematical and Physical Sciences, University of Technology Sydney, Ultimo, NSW 2007, Australia.

[b] School of Materials Engineering, Purdue University, 701 West Stadium Avenue, West Lafayette, IN 47907-2045, USA.

KEYWORDS. Nanodiamond, Oxidation, Thermal Stability, Size, Nitrogen-Vacancy (NV) Centre

Abstract

Oxidation has been suggested as an effective and scalable means for industrial purification of nanodiamond (ND) powders. However, conflicting accounts were reported with respect to oxidation behavior of commercial powders and the temperature range in which non-diamond phases can be removed efficiently. In this study, we investigate the effects of composition and structural characteristics of ND on the oxidation kinetics. The effect of crystal size was analyzed by directly measure the oxidation behavior of individual ND crystal in the size range 2-20 nm, probing the size-dependence of the oxidation kinetics at the lower end of the nanoscale. This study also leads to the first experimental data on the minimum size at which ND crystals become thermodynamically unstable and cease to exist as well as the minimum size of a luminescent ND still hosting an optically active nitrogen-vacancy (NV) center.

[*] Corresponding author. Tel: +61 029 514-2203. E-mail: carlo.bradac@uts.edu.au (Carlo Bradac)

1. Introduction

Nanocrystalline diamond, often simply referred to as nanodiamond (ND), has stirred rapidly growing interest during recent years, particularly in the forms of ultra-dispersed diamond (UDD) and detonation nanodiamond (DND). It combines the favorable mechanical, thermal, electrical and optical properties of bulk diamond with the high surface area and chemical reactivity of nanomaterials [1-3]. Owing to these unique characteristics and the availability of several, relatively simple processes for its synthesis, ND has become one of only few nanomaterials produced on an industrial scale [4, 5]. Current uses comprise electroplating baths [6], catalyst support [7], additive for composite materials [7-11], lubricants [12], and cooling fluids [13]. At the same time, NDs containing color centers such as the nitrogen-vacancy (NV) center [14] have been proposed and utilized as ideal solid-state spin quantum bits [15], high-resolution nanoscale sensors for measuring electric fields [16], magnetic fields [17-19] and temperature [20], as well as suitable bio-labels for optical trapping [21], bioimaging [22-24] and drug delivery [25-27] in biomedical applications.

A major drawback of bulk synthesis methods, such as detonation, is the limited control over structural uniformity and composition of the produced nanomaterial. In the case of ND, the detonation process yields a powder containing up to 80 wt% of non-diamond species [4, 5]. The resulting detonation soot is primarily composed of amorphous and graphitic carbon, which prevents a direct use of the as-produced powders and makes purification one of the most crucial steps in ND production. In order to overcome the well-known challenges associated with liquid-phase purification methods [28], researchers have explored a variety of gas-phase methods [29-35]. In particular, oxidation in air was found to be an economically feasible alternative to currently-employed methods as it provides a simple and efficient route to selectively remove non-diamond carbon and other impurities from the as-produced material [28, 31, 33, 36-42]. Purity levels as high as 96 wt% were reported without notable losses in the diamond phase in the temperature range 400-430 °C [38]. While other studies yielded similar results [40], some authors reported higher temperatures for the selective removal of non-diamond carbon. Tyurnina et al. recommended oxidation temperatures as high as 550 °C [41], while Cataldo et al. found that ND powders were stable towards oxidation below 450 °C, but burn rapidly above this temperature [43]. While the above studies have successfully demonstrated the great potential of air oxidation in ND processing, they also reveal the need for a better understanding of the oxidation behavior of ND powders.

Oxidation has also been discussed as means to control the crystal size in ND powders. This is important as many of the proposed nanodiamond-based technologies rely on specific material requirements with size being one of the most crucial ND properties. For instance, NV-center-based, single-spin magnetometry and Förster resonance energy transfer (FRET), depend strongly on the interaction radius r ($1/r^3$ [17] and $1/r^6$ [44], respectively). Small fluorescent NDs are also desirable for biological imaging and nanomedicine applications where the reduced ND size would minimize the disruption to the molecular trafficking under observation [22] and could ultimately lead to probing single molecules, individually [45, 46]. Mohan et al. demonstrated that the size of individual ND crystals (size range 20-50 nm) could be reduced by air oxidation above 500 °C. In contrast, Osswald et al. reported that upon direct oxidation in air, the average crystal size of ND powders increased [47, 48].

The inconsistencies in the reported oxidation behavior of ND result primarily from differences in structure and composition of commercially available powders [41]. In this study, we systematically investigate the effect of composition, structure, and crystal size on the oxidation mechanism of NDs. Moreover, for the first time, we directly probe the oxidation behavior of individual ND crystals in the size range 2-20 nm, providing experimental proof of the size-dependence of thermal stability of ND in oxidative environments.

2. Experimental

2.1 Oxidation of Bulk Powders

Detonation ND powders (UD50, UD90 and UD98) were supplied by NanoBlox, Inc. (USA). Black UD50 is the raw detonation soot. UD90 (acid oxidation) and UD98 (extensive acid oxidation) samples were prepared by different multistage acid purifications using nitric and sulfuric acid. Air oxidation was conducted for 5h at 425 °C in a closed tube furnace in static air at atmospheric pressure.

2.2. Raman Spectroscopy and Thermogravimetric Analysis

UV Raman spectra were recorded using a Renishaw 2000 Raman Microspectrometer with a 325-nm HeCd laser (3.81 eV, 2400 l/mm grating, 15x/40x objective, max. 1300 W/cm^2) and a 100 cm^{-1} cut-off notch filter. Data analysis was performed using GRAMS-32 and WiRE 2.0 software from Renishaw.

Thermogravimetric analysis (TGA) was performed using a SDT 2960 DTA-TGA from TA instruments and a Perkin Elmer TGA 7. In all experiments a gas flow of 40 ml/min was applied. Specimen powders (5-10 mg) were placed on a platinum pan, loaded into the instrument, and subsequently heated from 25 to 800 °C at 2 °C/min.

2.3 Oxidation of individual ND crystals and AFM measurements

The material used in this series of experiments was ND powder synthesized by the high pressure high temperature (HPHT) method and supplied by Microdiamant (MSY, <0.1 μm). For analysis, the ND were dispersed on a glass coverslip where a 5×5 unit grid consisting of 50×50 μm^2 squares had been previously laser scribed [49]. The as-received ND powder was first processed by a multiple-step acid cleaning procedure, to remove non-carbon impurities [49-51]. Purified NDs were then dispersed on a borosilicate BK7 glass coverslip (dimensions 22×22 mm^2, thickness (150±20) μm, BB022022A1; Menzel-Glaser). The coverslip was sonicated and rinsed in acetone (C_3H_6O, purity ≥99.5%; Sigma-Aldrich) for 10 minutes before the NDs were dispersed. Size and fluorescence of the NDs were examined simultaneously via a lab-built confocal microscope integrated with an atomic force microscope (Ntegra; NT-MDT), as described in Ref. [52]. The confocal-sample scanning fluorescence microscope (100× oil immersion objective lens with NA 1.3) employed an excitation 532-nm CW diode pumped solid-state laser (Compass 315-M100; Coherent). The fluorescence of the nanodiamonds and the intensity autocorrelation curves $g^{(2)}(\tau)$ were measured by a Hanbury-Brown and Twiss interferometer consisting of two avalanche photodiodes (SPCM-AQR-14; Perkin Elmer) and a correlator (PicoHarp 300, TCSCP System, 4-ps channel width, with digital and analog units PH 300; PicoQuant).

Air oxidation was conducted in a furnace (KSL-1100X-S Compact Muffle Furnace; MTI Corporation) at atmospheric pressure. Two different cycles with multiple, consecutive 30-min oxidation steps, were carried out separately at 500 °C and 430 °C. A preliminary oxidation for 3 hours at 600 °C was performed on the acid-treated ND samples for the further removal of tight graphitic and amorphous carbon layers surrounding the ND cores and left unaffected by the acid treatment [49, 53]. The size (height) of the NDs after each oxidation step was obtained from Atomic Force Microscope (AFM) scan topographies by fitting each crystal with 2-dimensional Gaussians, after the subtraction of the background height offset (cf. SI, Fig. S1b)

3. Results and discussion

3.1 Structure and Composition of Nanodiamond Powders

The as-produced DND powders collected from the detonation chamber contain a wide variety of carbon materials (>70 wt%) alongside the ND crystals, including amorphous carbon, carbon onions, nanocrystalline graphite and graphene nanoribbons. Non-carbonaceous impurities include trace amounts of metals (e.g. Fe, Al, Ca, Mg, Zn, Cu) and non-metal species (e.g. H, N, O, S), which exist primarily in the form of surface functional groups. The exact composition of commercial ND powders and their purity levels can vary substantially (23-95 wt.% sp^3) and are strongly dependent on the chemical history of the sample (i.e. synthesis and purification conditions).

Figure 1a shows the Raman spectra of three ND powders with different purity levels. Low-purity ND powders are dark in color or even black, as in the case of the unpurified detonation soot. Due to the large content of sp^2 species, their Raman spectra are dominated by the graphitic D and G Raman bands centered around 1400 and 1600 cm^{-1} (325-nm laser excitation), respectively. In contrast, purified ND powders appear lighter in color and exhibit a notable diamond Raman peak, asymmetrically broadened and downshifted to ~1325 cm^{-1} due to the confined diamond crystal size. The average crystal diameter in detonation ND measures only 4-5 nm; however, crystals as large as 50 nm can be found in the powders [54]. The majority of ND crystals exhibit high crystallinity, but twins, stacking faults and other dislocations are observed and likely contribute to the observed line broadening [55].

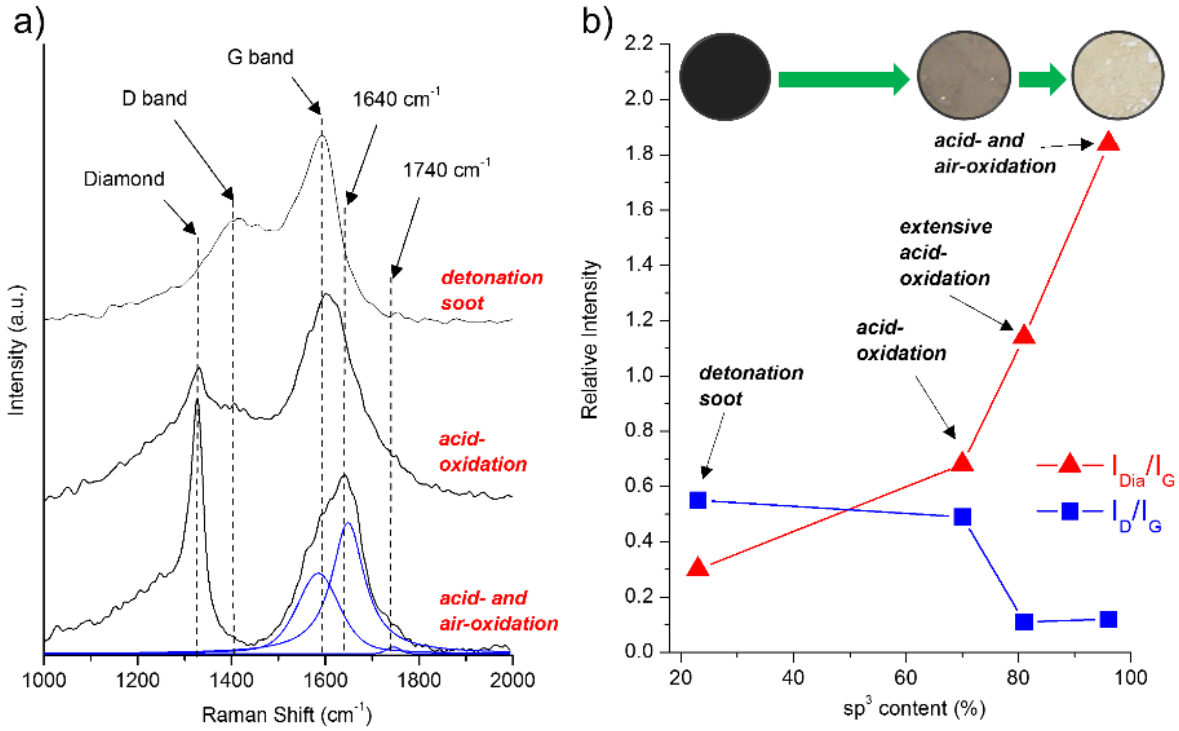

Figure 1. a) Raman spectrum (325-nm laser excitation) of ND powders with different levels of purity. The graphitic (sp^2) D and G bands (1400 and 1600 cm^{-1}, respectively) dominate the spectrum in low-purity ND powders (top trace), whilst the diamond Raman peak (downshifted at ~1325 cm^{-1}) clearly emerges in purified ND powder (bottom trace). **b)** Relative intensity of diamond peak against non-diamond Raman features. The ratio strongly depends on the purity (i.e. sp^3 content) of the sample.

The relative intensity of the diamond peak with respect to the non-diamond Raman features is strongly dependent on the purity (sp^3 content) of the sample (Fig. 1b). Of particular interest is the intensity ratio between diamond peak and G band Raman (I_{Dia}/I_G), as it can serve as a fast and inexpensive measure of the diamond (sp^3) content in the ND powders, in analogy to the I_D/I_G intensity ratio used to evaluate the disorder in graphitic carbons [56]. The I_D/I_G ratio in ND powder decreases with increasing sp^3 content as D band originates from the breathing modes of the hexagonal carbon rings in graphitic carbons, whereas the G band results from in-plane vibrations of the sp^2-bonded carbon atoms. However, great care must be taken with this analysis as the "G band" of purified ND powders is more complex and contains significant contributions from surface functional groups such as O-H (1640 cm^{-1}) and C-O (1740 cm^{-1}), as shown in Fig 1a [55]. Oxidation removes non-diamond carbon impurities, which encapsulate the ND crystals in low-purity powders, and subsequently saturate the diamond surface with oxygen-containing carbonyl and carboxyl groups. These changes in composition render the ND powder increasingly hydrophilic, leading to increased moisture adsorption and further increase in the O-H Raman signal. The

exact composition (e.g. quantity and type of functional groups) of the ND surface chemistry is strongly dependent on the oxidation treatment as well as the prevailing reaction conditions used for ND purification.

3.2 Oxidation Kinetics

The oxidation of carbon materials consists of several steps, any of which can become the rate limiting process: diffusion of oxygen 1) to the outer surface of the carbon particle and 2) through pores/cavities, 3) adsorption of oxygen (physisorption), 4) formation of oxygen-carbon bonds (chemisorption), 5) breaking of carbon-carbon bonds, 6) desorption of reaction products, and diffusion of reaction products through 7) pores/cavities and 8) away from the carbon particle. The relative contribution of each step to the overall reaction kinetics depends on the temperature, concentration of the oxidizing species, active surface area, amount of catalyst impurities and surface functionalities, diffusion constants, and/or number of defects.

At low temperatures, referred to as the chemical regime, the concentration of the oxidant is essentially the same everywhere in the sample and reaction rates are largely determined by the intrinsic reactivity of the carbon material. In this case, the rate controlling processes are steps 3-6. The chemical regime ranges from approximately 300 to 600 °C, whereas different parts of the sample may react at different rates, depending on their structure. At higher temperatures, the reaction kinetics are increasingly dominated by mass transport processes. In most cases, however, oxidation reactions occur mainly in the chemical regime and are, in a first approximation, independent from the diffusion of oxidants and reactants.

Although the oxidation kinetics of macroscopic forms of carbon, such as diamond and graphite [57-60], have been studied extensively and are well understood, in the case of nanomaterials, the mechanisms involved become more complex as the structural variety yields a large number of energetically different reaction sites [61]. Size and surface effects become dominant and diffusion processes often affect oxidation kinetics at temperatures well below 600 °C [62].

In the chemical regime, the thermodynamically favored reaction between carbon and oxygen is the formation of CO_2 (first order reaction) [63, 64]. The rate at which the reaction progresses depends directly on the changes in concentration of the reactants according to:

$$-\frac{d[C]}{dt} = -\frac{d[O_2]}{dt} = \frac{d[CO_2]}{dt} = k[O_2]^n, \tag{1}$$

where $[C]$, $[O_2]$, and $[CO_2]$ are the concentration of carbon, oxygen, and carbon dioxide, respectively; k is the reaction rate constant, t is the time, and n is a numerical index that characterizes the order of the reaction ($n = 1$ for first order reactions) [65]. The temperature-dependence of k is given by the Arrhenius equation:

$$\ln k = \ln A - \frac{E_A}{R} \cdot \frac{1}{T}, \tag{2}$$

where T is the temperature (in K), R is the universal gas constant, E_A is the activation energy (in kJ/mol), and A is a pre-exponential constant, also known as frequency factor. The activation energy reflects the energy barrier that needs to be overcome to initiate the chemical reaction between C and O_2. In simplified reaction rate models such as this, the activation energy summarizes all temperature dependencies, including that of diffusion coefficients or sorption equilibrium constants, if not accounted for separately. The frequency factor A is a measure of the number of molecules that possess the required activation energy.

The change in concentration of the reactants can be measured by determining the weight change of the carbon sample during oxidation. Following the simplified power law in Eq. (1) and ignoring effects of volume or area changes on the reaction kinetics [66], the weight loss during oxidation is given by:

$$\frac{dm}{dt} = -k \cdot m, \tag{3}$$

where m is the sample weight and k is the reaction rate constant for a given temperature (isothermal reactions) [67]. The weight change during oxidation is commonly expressed in terms of the weight fraction, α, which for a highly porous material (no shape effects) is defined as:

$$\alpha = \frac{m_0 - m}{m_0} = -k \cdot t \tag{4}$$

Using Eqs. (2) and (4), the activation energy and frequency factor can then be determined from the Arrhenius curve:

$$\ln \alpha = \ln A + \ln t - \frac{E_A}{R} \cdot \frac{1}{T} \tag{5}$$

Under non-isothermal conditions, Eq. (5) is modified to account for temperature changes, yielding the Achar-Brindley-Sharp-Wendeworth (ABSW) equation:

$$\ln\left[\frac{1}{F(\alpha)}\cdot\frac{d\alpha}{dT}\right]=\ln\left(\frac{k_0}{\beta}\right)-\frac{E_A}{R}\cdot\frac{1}{T}, \tag{6}$$

where β is the heating rate, dα/dT is the oxidation reaction rate, and F(α) is a differential function describing the reaction mechanism. In the chemical regime, the oxidation process is well described by a first order reaction and F(α) = (1 – α) [62, 68]. The kinetic parameters can be determined by plotting ln [$d\alpha$/dT/(1 – α)] vs. 1/T.

For both isothermal and non-isothermal oxidation, changes in the slope of the Arrhenius-type curves indicate a change in the reaction mechanisms. At low temperatures, reactions are controlled by the chemical process itself, while at elevated temperatures (>600 °C) oxidation reactions are increasingly dominated by the diffusion of the active species. The critical temperature that separates both steps depends on several factors, including surface area and pore structure of the material [69], and has been neither well defined nor exactly determined, particularly for carbon nanomaterials [64]. Other critical factors are the concentration of the oxidizing agents, the flow and/or agitation rates used during the experiments, and mechanical stress applied to the material [64].

3.3 Oxidation of Bulk Powders

In this study, we compared the oxidation behavior of four ND powders with different purity levels using thermogravimetric analysis (TGA). Figures 2a and 2b show the weight fraction, α, and its first derivative, *dα/dT*, respectively. The corresponding ABSW plot (Fig. 2c) and the derived rate coefficients (Fig. 2d) are also depicted.

Because of the large structural variety contained in the sample, oxidation of the unpurified detonation soot occurs over a wide temperature range (350-550 °C), as shown in Fig. 2b. The high content of amorphous carbon causes the oxidation to start at temperatures as low as 350 °C, with the maximum weight loss taking place around 510 °C. The low temperature (LT) region is dominated by oxidation of non-diamond carbons (E_A=84 kJ/mol), whereas at higher temperatures (HT), oxidation kinetics are controlled by the diamond phase (E_A=205 kJ/mol).

Acid oxidation removes the majority of the amorphous and graphitic carbon impurities, leading to a higher overall activation energy of the sample (241 kJ/mol), thus shifting the onset of ND oxidation towards higher temperatures (~425 °C) and narrowing the oxidation range to 425-560 °C (Fig. 2b) . The maximum weight loss occurs at ~490 °C, which is lower than that of the as-received detonation soot. This discrepancy may be explained by the fact that in the case of the unpurified powders, amorphous and graphitic carbon enclose the ND crystals, protecting them against oxidation at the early stages of the reaction. After acid purification, NDs are exposed, shifting the onset of ND oxidation and maximum weight loss to lower temperatures.

Another important factor determining the oxidation behavior of ND powders is the content of metal impurities, as many of these metals are known to catalyze the carbon-oxygen reaction, particularly Fe. The detonation soot exhibits a higher Fe content (~1.3 wt%) as compared to the acid purified powder; however, the Fe particles are encapsulated in carbon shells and remain catalytically inactive at the early stages of the oxidation. In purified ND, acid-treatments have reduced the amount of Fe contained in the powders (~0.7 wt%), but the catalyst particles are accessible and lower the energy barrier (temperature) for carbon oxidation. Extensive acid-purification has been used to further reduce the Fe content to less than 0.3 wt%, which shifts both the onset of oxidation (~450 °C) and maximum weight loss (~540 °C) to higher temperatures. However, it should be noted that the various oxidation treatments may also alter the ND size distribution by selectively removing smaller ND crystals that exhibit lower resistance towards oxidation, which would ultimately increase the oxidation resistance of the ND powder.

Finally, it is important to consider the surface chemistry of the various samples as it directly affects ND properties such as wetting behavior, surface charge, agglomeration, adsorption, and chemical reactivity. The quantity and type of functional groups formed vary depending on the oxidation conditions and the reacting species. Acid oxidation (HNO_3, H_2SO_4) tends to yield more carboxylic groups, while gas phase oxidation result in a high concentration of carbonyl groups, which exhibit higher thermal stability [70]. This explains the higher oxidation resistance of ND powders that were treated by both acid- and air-oxidation, which contain similar amounts of Fe as compared to samples purified solely in acid (Fig. 2b). In ND powders that were first purified by conventional acid treatments, but subsequently oxidized in air, many of the carboxylic surface functionalities are converted to more thermally stable carbonyl, lactone, and phenol groups, thus increasing the oxidation temperature range (425-600 °C) and shifting the temperature of maximum weight loss to ~530 °C. The onset of oxidation is less affected as not all of the carboxylic surface groups are converted. More extensive, multistage acid purification was shown to yield a higher content of C-H groups, which are generally more resistant towards oxidation as compared to oxygen-containing surface group. While the higher onset (450 °C) and maximum weight loss

temperatures (540 °C) maybe ascribed to the lower Fe content or potential changes in the average crystal size, as compared to conventional acid treatments, the wider oxidation temperature range (450-610 °C) and the shoulder in *dα/dT* suggest that the surface chemistry also plays a critical role in the oxidation process.

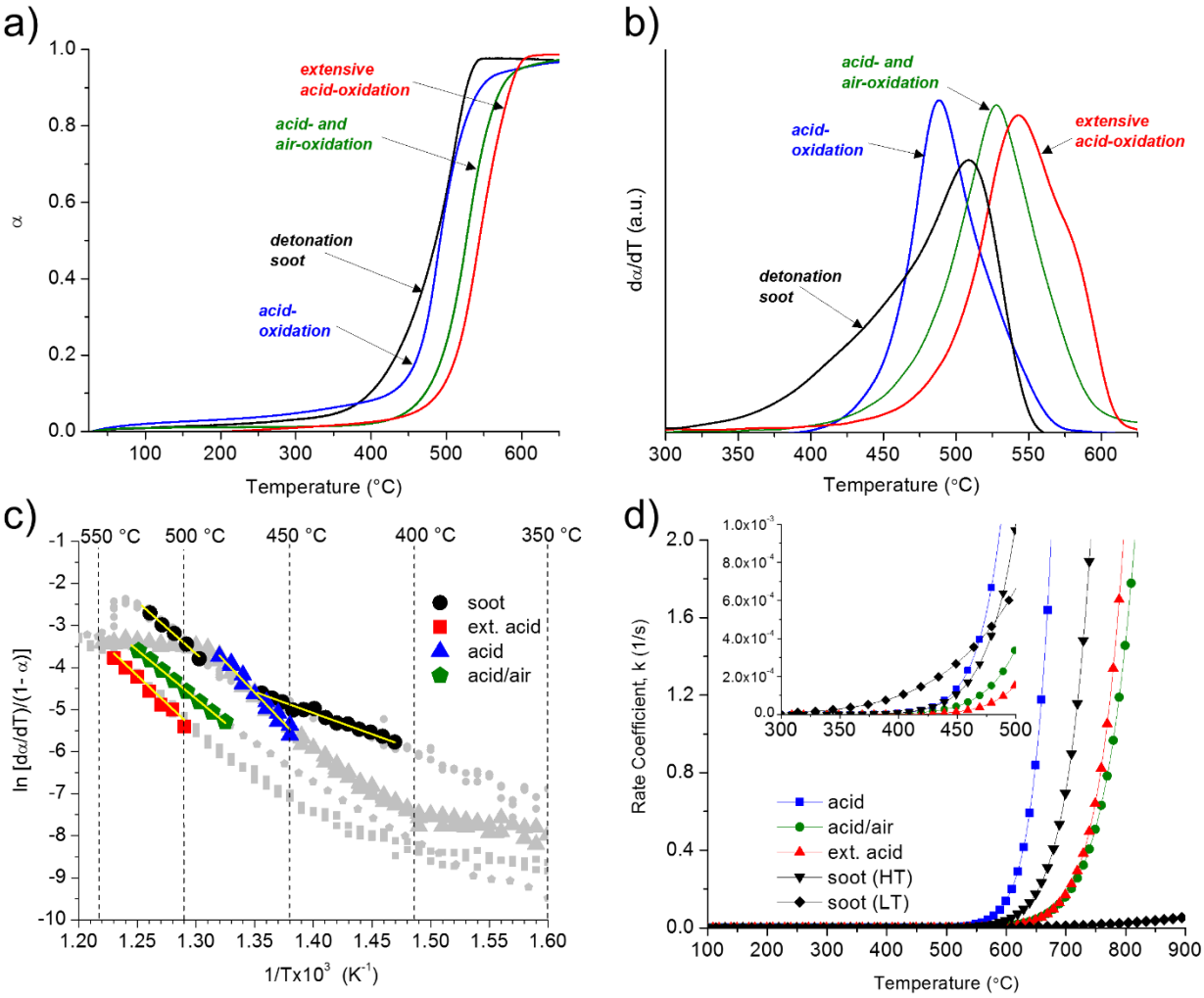

Figure 2. Thermogravimetric Analysis (TGA) of four ND powders with different levels of purity. **a, b)** Weight fraction, α, and its first derivative, *dα/dT*, respectively. **c)** Determination of the kinetic parameters of the powders via plotting of ln[*dα*/*d*T/(1 – *α*)] vs. 1/*T* [71, 72]. **d)** Dependence of the rate coefficient *k* vs temperature for the weight loss *dm/dt* during oxidation.

Table 1 summarizes the values for activation energy, E_A, frequency factor, A, and Fe content of the analyzed ND powders.

Table 1. Reaction kinetics parameters of ND powders

Sample	E_A **(kJ/mol)**	A **(1/sec)**	**Fe (wt%)**
acid	-243	4.3×10^{13}	0.68
ext. acid	-219	1.0×10^{11}	0.24
acid/air	-192	3.3×10^{9}	0.90
soot (HT)	-205.1	7.2×10^{10}	1.3
soot (LT)	-84	2.7×10^{2}	

Summary of the reaction kinetics parameters for the different ND powders we analyzed.

3.4 Oxidation of Individual Nanodiamonds

To gain deeper insight into the effect of size on the oxidation process at the low end of the nanoscale, we also investigated air oxidation of individual NDs in the size range 2-20 nm. The oxidation rate was determined by selecting individual, isolated crystals and measuring the reduction in size after several oxidation steps using a lab-built confocal microscope combined with an atomic force microscope (cf. SI, Fig. S1). Oxidation treatments were conducted at 430 °C and 500 °C, using multiple, consecutive isothermal oxidation steps (30 min/step) at both temperatures. For both experiments, a total of 150 individual NDs were selected and assigned to one of three characteristic size ranges (20-7 nm, 6-4 nm, and <4 nm). Figure 3a and 3b show the average size reduction for each of the three size ranges at 500 and 430 C, respectively. The corresponding numerical values are summarized in Table 2.

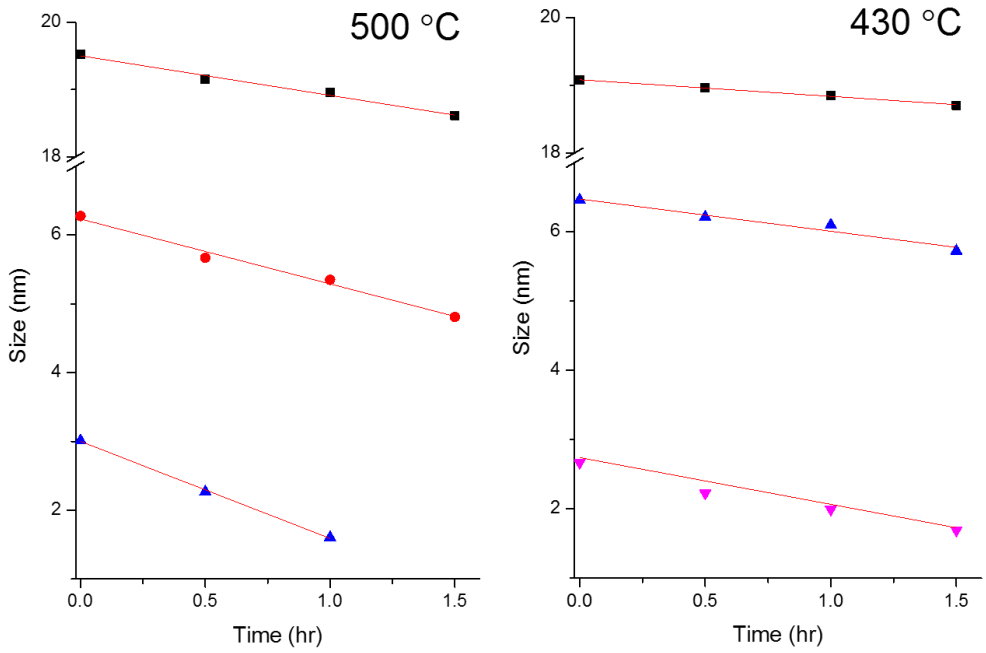

Figure 3. Air-oxidation etching rate of nanodiamonds at 500 °C and 430 °C. The etch rates are average values obtained from measuring the reduction in size over 3 to 4 consecutive oxidation steps of each of the 50 crystals selected for every size range (cf. SI, Fig. S1).

Table 2. NDs Size reduction

Temperature (^{o}C)	Size range (nm)	Etch rate (nm/h)
500	≤ 4	1.40±0.15
	6-4	0.95±0.15
	20-7	0.60±0.15
430	≤ 4	0.55±0.15
	6-4	0.40±0.15
	20-7	0.25±0.15

Summary of the size reduction of nanodiamonds at two different temperatures, 500 °C and 430 °C. The etch rates are average values obtained from measuring the reduction in size over 3 to 4 consecutive oxidation steps of each of the 50 crystals selected for every size range. The errors are the standard deviations of the measured etch rates for each population of crystals.

The results shown in Figure 3 and Table 2 suggest significant differences in oxidation rates depending on the actual size of the NDs. Smaller crystals etch faster than bigger crystals which seem to be more resilient to the air-oxidation process, which may be explained by the rapidly increasing surface-to-volume ratio at the lower end of the nanoscale. ND crystals with diameters about 4 nm have ~ 20% of the total number of atoms on the *surface*. This number changes to 50% for NDs in the size range around 3 nm [48].

Moreover, we measured a minimum critical size for the NDs of (1.60±0.35) nm (cf. SI, Fig. S1b). This value sets a threshold, suggesting that NDs smaller than that vanish "instantaneously" under the effect of air-oxidation or, in other words, that such a value of size is the minimum required for a diamond nanocrystal to exist. Finally, we investigated the optical properties of NV centers in small NDs. We measured the size and fluorescence of selected nanocrystals after every oxidation step to monitor their evolution. The smallest ND that we observed which still hosted an optically active NV^- center was (4.60±0.35) nm (cf. SI, Fig. S2). The phenomenon of blinking was also observed in a few fluorescent NDs [50, 73].

4. Conclusions

As with most carbon nanomaterials, as-produced ND powders are composed of mixtures of different nanoscale carbon structures, all of which exhibit different thermal stability and oxidation behavior. Depending on the purification history of the sample, diamond contents range from 25% (detonation soot) to more than 80% (acid-purified). The presence of different amounts of metal catalyst and large variations in surface chemistry further complicate the oxidation kinetics and must be taken into consideration when determining the oxidation (purification) conditions of commercial ND powders.

For the first time, we were able to investigate the oxidation behavior of individual ND crystals in the size range 2-20 nm and provide experimental data on the size-dependence of the oxidation kinetics at the lower end of the nanoscale. Our results show that small (<4 nm) ND crystals oxidize at much higher rates as compared to their larger (≥7 nm) counterparts, supporting our hypothesis that differences in oxidation kinetics lead to the observed upshift in the average crystal size in ND powders upon oxidation [48]. At the same time, we were able to measure the minimum size at which ND crystals become

thermodynamically unstable during oxidation and cease to exist. Finally, we provided experimental proof that there exists a minimum size of a luminescent ND still hosting an optically active nitrogen-vacancy (NV) center.

References

1. Mochalin, V.N., et al., *The properties and applications of nanodiamonds.* Nat Nano, 2012. **7**(1): p. 11-23.
2. Shenderova, O.A., V.V. Zhirnov, and D.W. Brenner, *Carbon Nanostructures.* Critical Reviews in Solid State and Materials Sciences, 2002. **27**(3-4): p. 227-356.
3. Krüger, A., *Carbon Materials and Nanotechnology* 2010: John Wiley & Sons.
4. Dolmatov, V.Y., *Ultradisperse diamonds of detonation synthesis: production, properties and applications* 2003, St. Petersburg: State Polytechnical University.
5. Gruen, D.M., O.A. Shenderova, and A.Y. Vul, eds. *Synthesis, Properties and Applications of Ultrananocrystalline Diamond*. NATO Science series. Series II: Mathematics, Physics and Chemistry. Vol. 192. 2005, Springer: Dordrecht, Berlin, Heidelberg, New York. 401.
6. Dolmatov, V.Y., *Detonation synthesis ultradispersed diamonds: properties and applications.* Russian Chemical Reviews, 2001. **70**(7): p. 607.
7. Su, D.S., S. Perathoner, and G. Centi, *Nanocarbons for the Development of Advanced Catalysts.* Chemical Reviews, 2013. **113**(8): p. 5782-5816.
8. Ohno, K., et al., *Engineering shallow spins in diamond with nitrogen delta-doping.* Applied Physics Letters, 2012. **101**(8): p. -.
9. Dreau, A., et al., *Avoiding power broadening in optically detected magnetic resonance of single NV defects for enhanced dc magnetic field sensitivity.* Physical Review B, 2011. **84**(19): p. 195204.
10. Oort, E.v., N.B. Manson, and M. Glasbeek, *Optically detected spin coherence of the diamond N-V centre in its triplet ground state.* Journal of Physics C: Solid State Physics, 1988. **21**(23): p. 4385.
11. Maitra, U., et al., *Mechanical properties of nanodiamond-reinforced polymer-matrix composites.* Solid State Communications, 2009. **149**(39â€“40): p. 1693-1697.
12. Red'kin, V.E., *Lubricants with Ultradisperse Diamond-Graphite Powder.* Chemistry and Technology of Fuels and Oils, 2004. **40**(3): p. 164-170.
13. Davidson, J.L. and D.T. Bradshaw, *Compositions with nano-particle size diamond powder and methods of using same for trasferring heat between a heat source and a heat sink*. 2005, Vanderbilt University: USA. p. 18.
14. Doherty, M.W., et al., *The nitrogen-vacancy colour centre in diamond.* Physics Reports, 2013. **528**(1): p. 1-45.
15. Jelezko, F., et al., *Observation of Coherent Oscillation of a Single Nuclear Spin and Realization of a Two-Qubit Conditional Quantum Gate.* Physical Review Letters, 2004. **93**(13): p. 130501.
16. Dolde, F., et al., *Electric-field sensing using single diamond spins.* Nat Phys, 2011. **7**(6): p. 459-463.
17. Balasubramanian, G., et al., *Nanoscale imaging magnetometry with diamond spins under ambient conditions.* Nature, 2008. **455**(7213): p. 648-651.
18. Maze, J.R., et al., *Nanoscale magnetic sensing with an individual electronic spin in diamond.* Nature, 2008. **455**(7213): p. 644-647.
19. Grinolds, M.S., et al., *Subnanometre resolution in three-dimensional magnetic resonance imaging of individual dark spins.* Nat Nano, 2014. **9**(4): p. 279-284.
20. Neumann, P., et al., *High-Precision Nanoscale Temperature Sensing Using Single Defects in Diamond.* Nano Letters, 2013. **13**(6): p. 2738-2742.
21. Geiselmann, M., et al., *Three-dimensional optical manipulation of a single electron spin.* Nat Nano, 2013. **8**(3): p. 175-179.
22. Chang, Y.-R., et al., *Mass production and dynamic imaging of fluorescent nanodiamonds.* Nat Nano, 2008. **3**(5): p. 284-288.
23. Mochalin, V.N. and Y. Gogotsi, *Wet Chemistry Route to Hydrophobic Blue Fluorescent Nanodiamond.* Journal of the American Chemical Society, 2009. **131**(13): p. 4594-4595.
24. Schrand, A.M., S.A.C. Hens, and O.A. Shenderova, *Nanodiamond Particles: Properties and Perspectives for Bioapplications.* Critical Reviews in Solid State and Materials Sciences, 2009. **34**(1-2): p. 18-74.
25. Shimkunas, R.A., et al., *Nanodiamond-insulin complexes as pH-dependent protein delivery vehicles.* Biomaterials, 2009. **30**(29): p. 5720-5728.
26. Purtov, K.V., et al., *Nanodiamonds as Carriers for Address Delivery of Biologically Active Substances.* Nanoscale Research Letters, 2010. **5**(3): p. 631 - 636.
27. Alhaddad, A., et al., *Nanodiamond as a Vector for siRNA Delivery to Ewing Sarcoma Cells.* Small, 2011. **7**(21): p. 3087-3095.
28. Petrov, I., et al., *Detonation nanodiamonds simultaneously purified and modified by gas treatment.* Diamond and Related Materials, 2007. **16**(12): p. 2098-2103.
29. Shenderova, O., et al., *Surface Chemistry and Properties of Ozone-Purified Detonation Nanodiamonds.* Journal of Physical Chemistry C, 2011. **115**(20): p. 9827-9837.
30. Pavlov, E.V. and Y.A. Skryabin, *Method For Removal Of Impurity Of Non-Diamond Carbon And Device For Its Realization*. 1994: Russia.
31. Mitev, D., et al., *Surface peculiarities of detonation nanodiamonds in dependence of fabrication and purification methods.* Diamond and Related Materials, 2007. **16**(4-7): p. 776-780.
32. Osswald, S., et al., *Control of sp(2)/sp(3) carbon ratio and surface chemistry of nanodiamond powders by selective oxidation in air.* Journal of the American Chemical Society, 2006. **128**(35): p. 11635-11642.
33. Xu, X.Y., et al., *Influence of surface modification adopting thermal treatments on dispersion of detonation nanodiamond.* Journal of Solid State Chemistry, 2005. **178**(3): p. 688-693.
34. Gubarevich, T.M., R.R. Sataev, and V.Y. Dolmatov. *Chemical purification of ultradisperse diamonds*. in *5th All-Union Meeting on Detonation*. 1991. Krasnoyarsk USSR.
35. Chiganov, A.S., *Selective Inhibition of the Oxidation of Nanodiamonds for Their Cleaning.* Physics of the Solid State, 2004. **46**(4): p. 595-787.

36. Gubarevich, T.M., R.R. Sataev, and V.Y. Dolmatov. *Chemical purification of ultradisperse diamonds* in *Proceedings of the 5th All-Union Meeting on Detonation*. 5-15 August 1991. Krasnoyarsk USSR.
37. Pavlov, E.V. and J.A. Skrjabin, *Method For Removal Of Impurity Of Non-Diamond Carbon And Device For Its Realization*. 1994: Russia.
38. Osswald, S., et al., *Control of sp2/sp3 carbon ratio and surface chemistry of nanodiamond powders by selective oxidation in air.* J. Am. Chem. Soc. , 2006. **128**: p. 11635-11642.
39. Chiganov, A.S., *Selective inhibition of the oxidation of nanodiamonds for their cleaning.* Physics of the Solid State, 2004. **46**(4): p. 620-621.
40. Kulakova, II, *Surface chemistry of nanodiamonds.* Physics of the Solid State, 2004. **46**(4): p. 636-643.
41. Tyurnina, A.V., et al., *Thermal purification of detonation diamond.* Journal of Surface Investigation-X-Ray Synchrotron and Neutron Techniques, 2010. **4**(3): p. 458-463.
42.], A.S.C., et al., *Method For Cleaning Detonation Diamonds* 1993: Russia.
43. Cataldo, F. and A.P. Koscheev, *A study on the action of ozone and on the thermal stability of nanodiamond.* Fullerenes Nanotubes and Carbon Nanostructures, 2003. **11**(3): p. 201-218.
44. Chen, Y.-Y., et al., *Measuring Forster resonance energy transfer between fluorescent nanodiamonds and near-infrared dyes by acceptor photobleaching.* Diamond and Related Materials, 2011. **20**(5-6): p. 803-807.
45. Fu, C.-C., et al., *Characterization and application of single fluorescent nanodiamonds as cellular biomarkers.* Proceedings of the National Academy of Sciences, 2007. **104**(3): p. 727-732.
46. Perunicic, V.S., et al., *Towards single-molecule NMR detection and spectroscopy using single spins in diamond.* Physical Review B, 2014. **89**(5): p. 054432.
47. Gordeev, S. and S. Korchagina, *On the stability of small-sized nanodiamonds.* Journal of Superhard Materials, 2007. **29**(2): p. 124-125.
48. Osswald, S., et al., *Increase of nanodiamond crystal size by selective oxidation.* Diamond and Related Materials, 2008. **17**(7-10): p. 1122-1126.
49. Gaebel, T., et al., *Size-reduction of nanodiamonds via air oxidation.* Diamond and Related Materials, 2011. **21**(0): p. 28-32.
50. Bradac, C., et al., *Observation and control of blinking nitrogen-vacancy centres in discrete nanodiamonds.* Nat Nano, 2010. **5**(5): p. 345-349.
51. Maletinsky, P., et al., *A robust scanning diamond sensor for nanoscale imaging with single nitrogen-vacancy centres.* Nat Nano, 2012. **7**(5): p. 320-324.
52. Bradac, C., et al., *Prediction and Measurement of the Size-Dependent Stability of Fluorescence in Diamond over the Entire Nanoscale.* Nano Letters, 2009. **9**(10): p. 3555-3564.
53. Osswald, S., et al., *Control of sp2/sp3 Carbon Ratio and Surface Chemistry of Nanodiamond Powders by Selective Oxidation in Air.* Journal of the American Chemical Society, 2006. **128**(35): p. 11635-11642.
54. Yushin, G.N., et al., *Effect of sintering on structure of nanodiamond.* Diamond and Related Materials, 2005. **14**(10): p. 1721-1729.
55. Osswald, S., et al., *Phonon confinement effects in the Raman spectrum of nanodiamond.* Physical Review B, 2009. **80**(7): p. 075419.
56. Ferrari, A.C. and J. Robertson, *Raman spectroscopy of amorphous, nanostructured, diamond–like carbon, and nanodiamond.* Philosophical Transactions of the Royal Society of London. Series A: Mathematical, Physical and Engineering Sciences, 2004. **362**(1824): p. 2477-2512.
57. Ulbricht, H., G. Moos, and T. Hertel, *Interaction of molecular oxygen with single-wall carbon nanotube bundles and graphite.* Surface Science, 2003. **532**: p. 852-856.
58. Giannozzi, P., R. Car, and G. Scoles, *Oxygen adsorption on graphite and nanotubes.* The Journal of Chemical Physics, 2003. **118**(3): p. 1003-1006.
59. Klusek, Z., et al., *Nanoscale studies of the oxidation and hydrogenation of graphite surface (vol 45, pg 1383, 2003).* Corrosion Science, 2004. **46**(7): p. 1831-1831.
60. Lee, S.M., et al., *Defect-induced oxidation of graphite.* Physical Review Letters, 1999. **82**(1): p. 217-220.
61. Chang, H.P. and A.J. Bard, *Scanning tunneling microscopy studies of carbon oxygen reactions on highly oriented pyrolytic graphite.* Journal of the American Chemical Society, 1991. **113**(15): p. 5588-5596.
62. Gao, P.Z., H.J. Wang, and Z.H. Jin, *Study of oxidation properties and decomposition kinetics of three-dimensional (3-D) braided carbon fiber.* Thermochimica Acta, 2004. **414**(1): p. 59-63.
63. Demidov, A.I. and I.A. Markelov, *Thermodynamics of reaction of carbon with oxygen.* Russian Journal of Applied Chemistry, 2005. **78**(5): p. 707-710.
64. Goto, K.S., K.H. Han, and G.R. Saintpierre, *A REVIEW OF OXIDATION-KINETICS OF CARBON-FIBER CARBON MATRIX COMPOSITES AT HIGH-TEMPERATURE.* Materials Science and Engineering, 1987. **88**: p. 347-347.
65. Brukh, R. and S. Mitra, *Kinetics of carbon nanotube oxidation.* Journal of Materials Chemistry, 2007. **17**(7): p. 619-623.
66. Illekova, E. and K. Csomorova, *Kinetics of oxidation in various forms of carbon.* Journal of Thermal Analysis and Calorimetry, 2005. **80**(1): p. 103-108.
67. Yin, Y., et al., *THE OXIDATION BEHAVIOR OF CARBON-FIBERS.* Journal of Materials Science, 1994. **29**(8): p. 2250-2254.
68. Yang, Y., F. He, and M. Wang, Tansu, 1998. **1**: p. 2-15.
69. Chang, H.W. and S.K. Rhee, *Oxidation of carbon derived from phenolic resin.* Carbon, 1978. **16**(1): p. 17-20.
70. Figueiredo, J.L., et al., *Modification of the surface chemistry of activated carbons.* Carbon, 1999. **37**(9): p. 1379-1389.
71. Achar, B.N.N., G.W. Brindley, and J.H. Sharp. *Kinetics and mechanism of dehydroxylation process. III. Applications and limitations of dynamic methods*. in *Proceedings of International Clay Conference (Jerusalem)*. 1966.
72. Sharp, J.H. and S.A. Wentworth, *Kinetic analysis of thermogravimetric data.* Analytical Chemistry, 1969. **41**(14): p. 2060-2062.
73. Bradac, C., et al., *Effect of the Nanodiamond Host on a Nitrogen-Vacancy Color-Centre Emission State.* Small, 2012: p. n/a-n/a.